coatings

MDPI

Article

Growth of $Zn_{1-x}Ni_xO$ Thin Films and Their Structural, Optical and Magneto-Optical Properties

Ihor Stolyarchuk [1,2,*], Oleh Kuzyk [1], Olesya Dan'kiv [1], Andrzej Dziedzic [3], Gennadiy Kleto [2], Andriy Stolyarchuk [1], Andriy Popovych [1] and Ivan Hadzaman [1]

[1] Department of Physics and Information Systems, Drohobych Ivan Franko State Pedagogical University, 82100 Drohobych, Ukraine
[2] Department of Physics of Semiconductors and Nanostructures, Chernivtsi National University, 58012 Chernivtsi, Ukraine
[3] College of Natural Sciences, University of Rzeszow, 35959 Rzeszow, Poland
* Correspondence: i.stolyarchuk@dspu.edu.ua

Abstract: The radio frequency (RF) reactive sputtering technique has been used to prepare $Zn_{1-x}Ni_xO$ thin films with $0 \leq x \leq 0.08$. Composite targets were obtained by mixing and pressing NiO and ZnO powders. Sapphire, quartz and glass were used as substrates. X-ray diffraction analysis of Ni-doped ZnO films indicates that all samples are crystalised in a hexagonal wurtzite structure with a preferred orientation along the (002) plane. Any secondary phase, corresponding to metallic nickel clusters or nickel oxides was not observed. High-resolution transmission electron microscopy (HR-TEM) image observed for $Zn_{1-x}Ni_xO$ thin film shows a strong preferred orientation (texture) of crystalline columns in the direction perpendicular to the substrate surface. Different surface morphology was revealed in AFM images depending on the film composition and growth condition. Optical absorption spectra suggest the substitution of Zn^{2+} ions in the ZnO lattice by Ni^{2+} ions. The energy bandgap value was also found a complex dependence with an increase in Ni dopant concentration. In photoluminescence spectra, two main peaks were revealed, which are ascribed to near band gap emission and vacancy or defect states. Faraday rotation demonstrates its enhancement and growth of ferromagnetism with the increase in Ni content of $Zn_{1-x}Ni_xO$ thin films at room temperature.

Keywords: ZnNiO thin films; rf reactive sputtering technique; optical absorption; photoluminescence; Faraday rotation; ferromagnetism

Citation: Stolyarchuk, I.; Kuzyk, O.; Dan'kiv, O.; Dziedzic, A.; Kleto, G.; Stolyarchuk, A.; Popovych, A.; Hadzaman, I. Growth of $Zn_{1-x}Ni_xO$ Thin Films and Their Structural, Optical and Magneto-Optical Properties. *Coatings* **2023**, *13*, 601. https://doi.org/10.3390/coatings13030601

Academic Editor: Panos Poulopoulos

Received: 28 January 2023
Revised: 28 February 2023
Accepted: 6 March 2023
Published: 11 March 2023

1. Introduction

In recent years, zinc oxide-based diluted magnetic semiconductors (DMSs) attract much attention because of their unique characteristics and as a kind of potential material for spintronic applications. Theoretical prediction of ferromagnetism [1,2] above room temperature in transition metal (TM)-doped ZnO-based DMSs was the additional stimulus for much experimental and theoretical research of these materials. However, if some researchers reported that the TM-doped ZnO showed room temperature ferromagnetism [3–9], the others have not observed such magnetic behaviour [10–13]. In the particular case of the Ni-doped ZnO films, Wakano et al. [14] have observed ferromagnetism at 2 K and superparamagnetism at 300 K. Ferromagnetism was observed at room temperature in the Ni-doped ZnO films [15–17]. The paramagnetism in the ZnO:Ni films was reported earlier by Yin et al. [18]. Thus, as follows from the literature, different magnetic properties for the nickel-doped ZnO system are reported. In this case, the factors leading to magnetism in nickel-doped ZnO are still not clear and require careful study. No doubt, the magnetic properties of ZnO-based DMSs depend significantly on growth technique. Different growth techniques such as MO-CVD, magnetron sputtering, chemical vapour deposition, spray pyrolysis, pulsed laser deposition, etc., have been used for preparing ZnO and TM-doped ZnO DMSs thin films. Among

these methods, RF reactive sputtering technique is less studied. Savchuk et al. [19–22] have demonstrated paramagnetic behaviours of ZnMnO thin films and ferromagnetic ordering in co-doped quaternary ZnMnFeO oxides prepared by RF sputtering.

In this work, we report on the preparation of $Zn_{1-x}Ni_xO$ thin films by RF reactive sputtering technique and examination of the changes in their structural, optical and magneto-optical properties depending on the nickel content within $0.00 \leq x \leq 0.08$.

2. Experimental Section

Thin films of $Zn_{1-x}Ni_xO$ were obtained by us by the method of RF reactive sputtering. We used quartz, sapphire and glass as substrates for sputtering. The sputtering process was carried out in an active gas medium was consist of are mixture of argon and oxygen. The composite targets with a diameter r of 70 mm were formed by mixing and pressing ZnO and NiO powders with appropriate rations of components. The sputtering process was carried out at a distance from the target to the substrate of 35 mm. The base vacuum in the chamber was maintained equal to 2×10^{-4} Pa, and the pressure of the working gas was 0.2 and 0.8 Pa for oxygen and argon, respectively. Sputtering was carried out at an input RF power of 300 W and a deposition rate of 10 nm/min. During deposition, the temperature of the substrate was 350–400 °C. After deposition, the samples were annealed in an oxygen atmosphere at a temperature of 500–550 °C.

The crystallographic studies were performed using X-ray diffractometer (D8 ADVANCE X-ray Diffractometer with DAVINCI) using Cu-K_α wavelength ($\lambda = 1.54059$ Å) and scanning in 2θ range from 10° to 70°. The high-resolution transmission electron microscopic (HR-TEM) images were recorded on the samples using the Tecnai Osiris X-FEG S/TEM microscope. Surface analysis of the samples was performed by atomic force microscopy in dynamic mode (non–contact) with force constant K ~ 40 N/m and f_0 ~ 300 kHz.

Optical absorption and photoluminescence (PL) spectra in range 350–600 nm were measured using a grating monochromator, a photodetector system and registered computer system. An excitation wavelength of 325 nm with intensity value of 10 mW (He-Cd laser) was chosen to record the PL intensity in this wavelength region, at room temperature.

Magneto-optical studies of the Faraday effect (experimental measurements of the rotation angle) in thin films and nanosized semiconductor structures deposited on relatively thick substrates are a rather problematic task [23].

In our studies, the experimental measurement of the Faraday angle (Faraday effect) was carried out using a specially designed setup described in [24]. A monochromatic beam of light after passing through a focusing lens and a polariser (Rochon prism) becomes linearly polarised and falls on a thin film under study, which is in an electromagnet with a magnetic field of up to 5 T. The analyser (Wollaston prism) located in the path of the light beam divides it into two beams passing through the modulator, which makes it possible to ensure their phase shift by 180°. In the absence of a magnetic field, the intensities of the two light beams are completely balanced. When the electromagnet is turned on, the resulting asymmetric signal is recorded using a system that includes a photomultiplier, a synchronised amplifier and a personal computer. Extracting of Faraday rotation angle for thin films was made by measuring the rotation angle from part of substrate which was not covered in oxide film. The developed setup makes it possible to investigate the angle of rotation with an accuracy of 10^{-4} rad.

3. Results and Discussion

The obtained X-ray diffraction (XRD) patterns of the pure ZnO and Ni-doped ZnO films showed that all as-grown samples are nanostructured polycrystalline films (Figure 1). The positions of all intense peaks can be assigned to the hexagonal wurtzite structure of the ZnO crystal with a (002) preferred orientation. As shown in Figure 1, with an increase in the Ni content above 2% ($x > 0.02$), additional diffraction peaks corresponding to (100), (101) and (102) orientations were observed. In addition, the relational intensity of the main (002) peak in the nickel concentration range $0 \leq x \leq 0.08$ is significantly higher than that of

the other peaks. At the same time, a significant result is the absence of peaks corresponding to metallic nickel clusters or nickel oxides. The obtained results designate that Ni^{2+} enters the ZnO lattice without changing the wurtzite structure and systematically replaces the Zn^{2+} ions in the lattice. This result indicates a preferential texture growth along the C axis in the studied films. Along with this, an increase in the concentration of nickel causes an increase in the intensity of all observed diffraction peaks, which can be explained by the refinement and improvement of the crystalline quality of these films due to doping with nickel. Using the obtained results, namely the full width at half maximum (FWHM) of the diffraction peak and the diffraction angle θ, the average crystallite size D was calculated using the Debye–Scherer's formula [25]:

$$D = \frac{0.9\,\lambda}{\Delta\theta\cos\theta} \quad (1)$$

where θ is the Bragg angle of the diffraction peak, Δθ is the FWHM and λ is the X-ray wavelength.

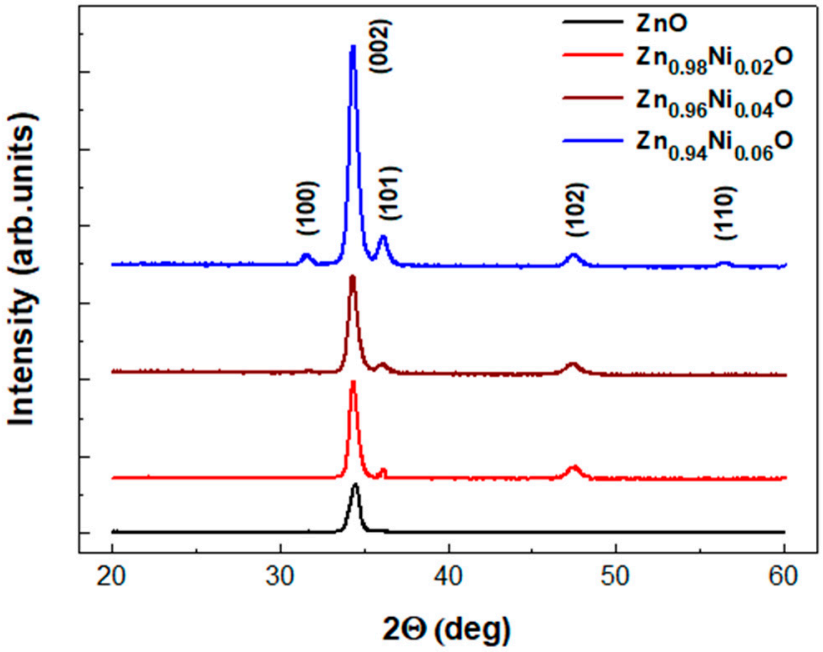

Figure 1. X-ray diffraction spectra of $Zn_{1-x}Ni_xO$ films with different Ni contents (x).

The calculation results indicate a decrease in the crystallite size with an increase in the nickel concentration. The same behaviour was observed for ZnO:Ni [26] and ZnO:Al [27] thin films. Obviously, the introduction of Ni atoms into the ZnO structure and an increase in their concentration determines the preferential location of the dopant atoms in the regions of grain boundaries or near them, which determines the decrease in the crystallite size. The lattice constants **a** and **c** for the samples of $Zn_{1-x}Ni_xO$ films were calculated using the Formula (2) and (3) [28] and depicted in Figure 2:

$$\frac{1}{d^2_{(h,k,l)}} = \frac{4}{3}\left(\frac{h^2+hk+k^2}{a^2}\right) + \frac{l^2}{c^2} \quad (2)$$

where $d_{h,k,l}$ is the interplanar spacing obtained from Bragg's law, a and c are the required lattice constants and h, k and l are the Miller indices denoting the plane. Equation (2) becomes:

$$a = \frac{\lambda}{\sqrt{3}\sin\theta}\,,\; c = \frac{\lambda}{\sin\theta} \quad (3)$$

under the first-order reflection (n = 1) on the (100) and (002) planes.

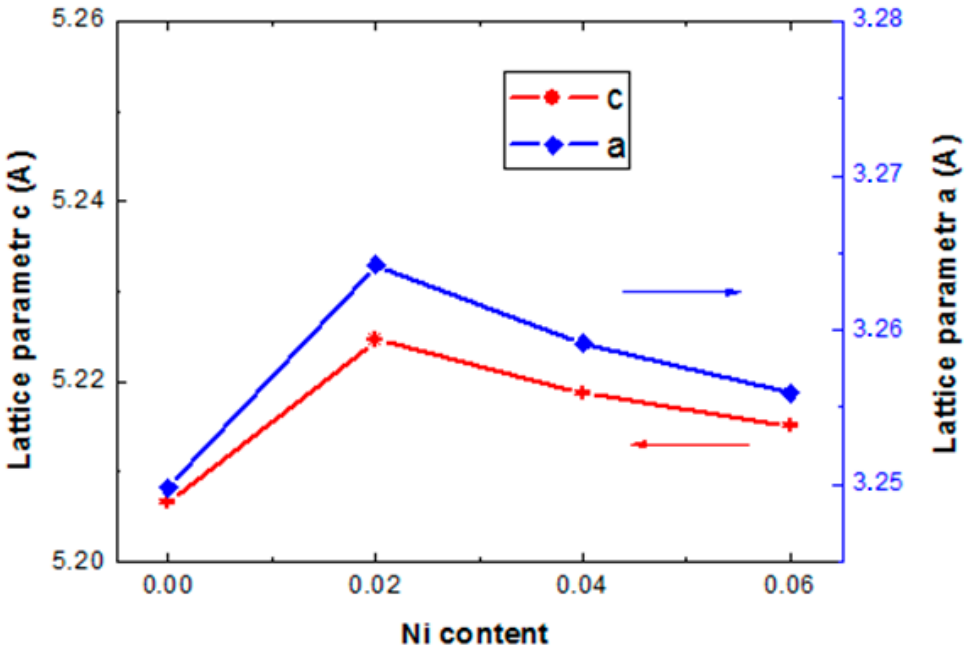

Figure 2. Dependence of the lattice parameters "a" and "c" on the increasing Ni content (x) in $Zn_{1-x}Ni_xO$ films.

The obtained results indicate an increase in the lattice parameters of deposited $Zn_{1-x}Ni_xO$ films for a nickel content of x = 0.02 and their decrease with a further increase in the concentration of Ni (x > 0.02). Taking into account the fact that the size of Ni^{2+} is 0.055 nm and is close to the size of Zn^{2+} in the tetrahedral configuration (equal to 0.06 nm) [29], Ni^{2+} ions systematically replace Zn^{2+} ions without changing the crystal structure.

Figure 3a,b shows cross-sectional images obtained by HR-TEM of the studied samples. As can be seen, all samples exhibit a columnar structure along the growth direction. In addition, this structure is dense and evenly textured. Energy dispersive X-ray detection (EDX) maps corresponding to the selected area in Figure 3b are shown in Figure 3c. The results indicate the presence of the elements Zn, Ni and O and do not contain other impurity elements, except for Cu and C (from the grid and not shown here). In addition, the data obtained indicate that Ni is evenly distributed in the film and forms a solid solution with the ZnO matrix.

As evidenced by the results of studying the surface of films, used by the AFM method, the growth conditions and oxide composition have a significant effect on its morphology. Figure 4 shows two-dimensional (2D) and three-dimensional (3D) AFM images for a 5 × 5 μm area measured by non-contact mode. It was revealed that compared with pure ZnO films, Ni doping leads to an increase in surface roughness. In addition, as can be seen from Figure 4, the surface of the $Zn_{1-x}Ni_xO$ films consists of a mixture of columnar and granular microstructures. Similar microstructures in AFM images recently were reported for Ni-doped ZnO films prepared by magnetron sputtering [30–32], sol–gel spin coating method [33–35] and pulsed laser deposition [36]. In particular, Gao et al. [30] showed that surface roughness is affected by the oxygen partial pressure.

According to these results [30,32] the root mean square (RMS) of the studied films was decreased when doped with Ni. Estimation of the R_{RMS} in our study demonstrates opposite results. For the films with Ni content of x = 0.02 the average roughness R_{RMS} = 35.5 nm, whereas for the films with Ni content of x = 0.06 this parameter is larger R_{RMS} = 65.7 nm. The results of AFM studies of all samples also indicate the growth of columns perpendicular to the plane of any substrate used.

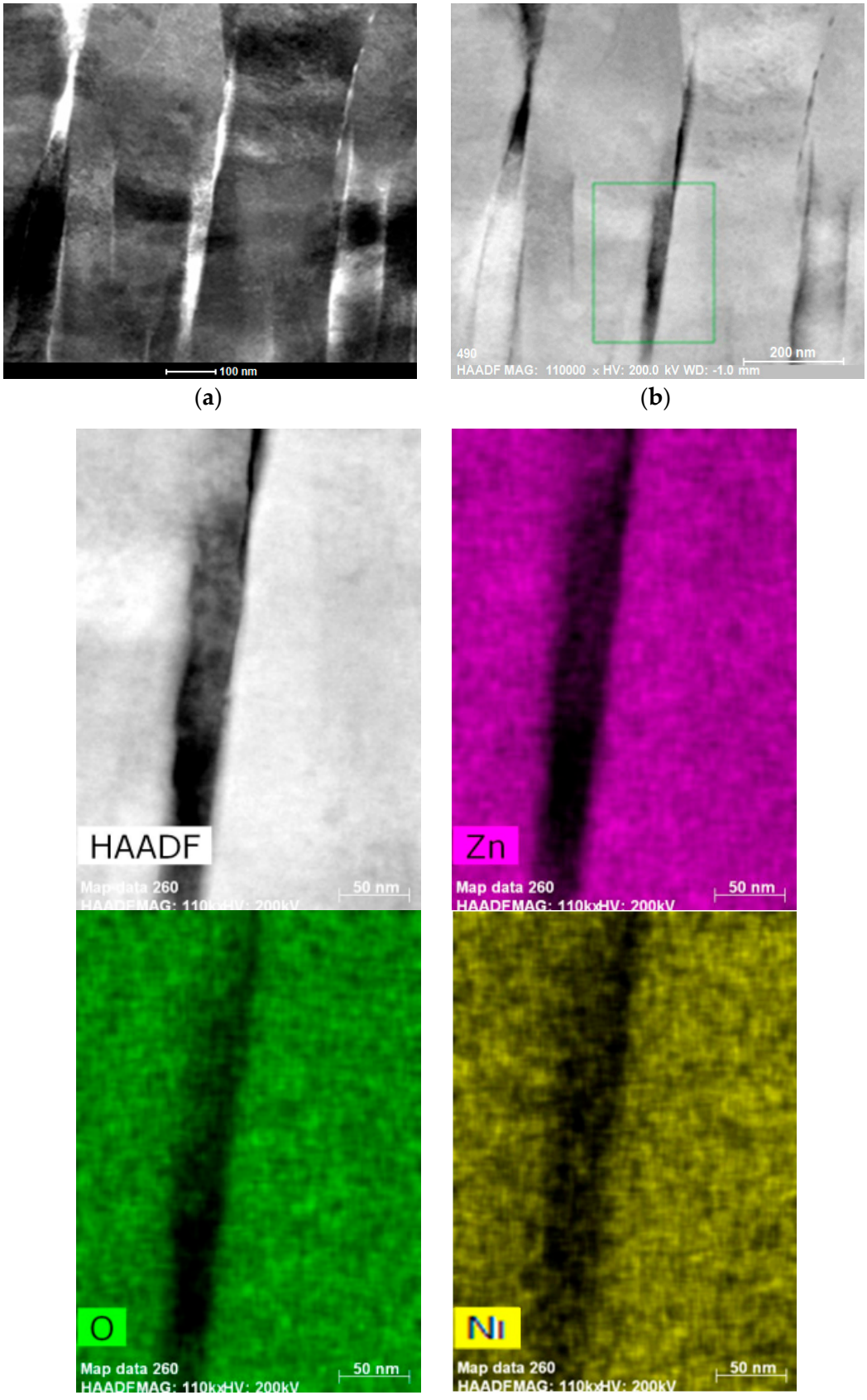

Figure 3. (**a**) STEM BF and STEM HAADF (Z–kontrast); (**b**) images of $Zn_{0.96}Ni_{0.04}O$ thin films; (**c**) EDX analysis confirms the presence of nickel in the ZnO matrix in the selected area.

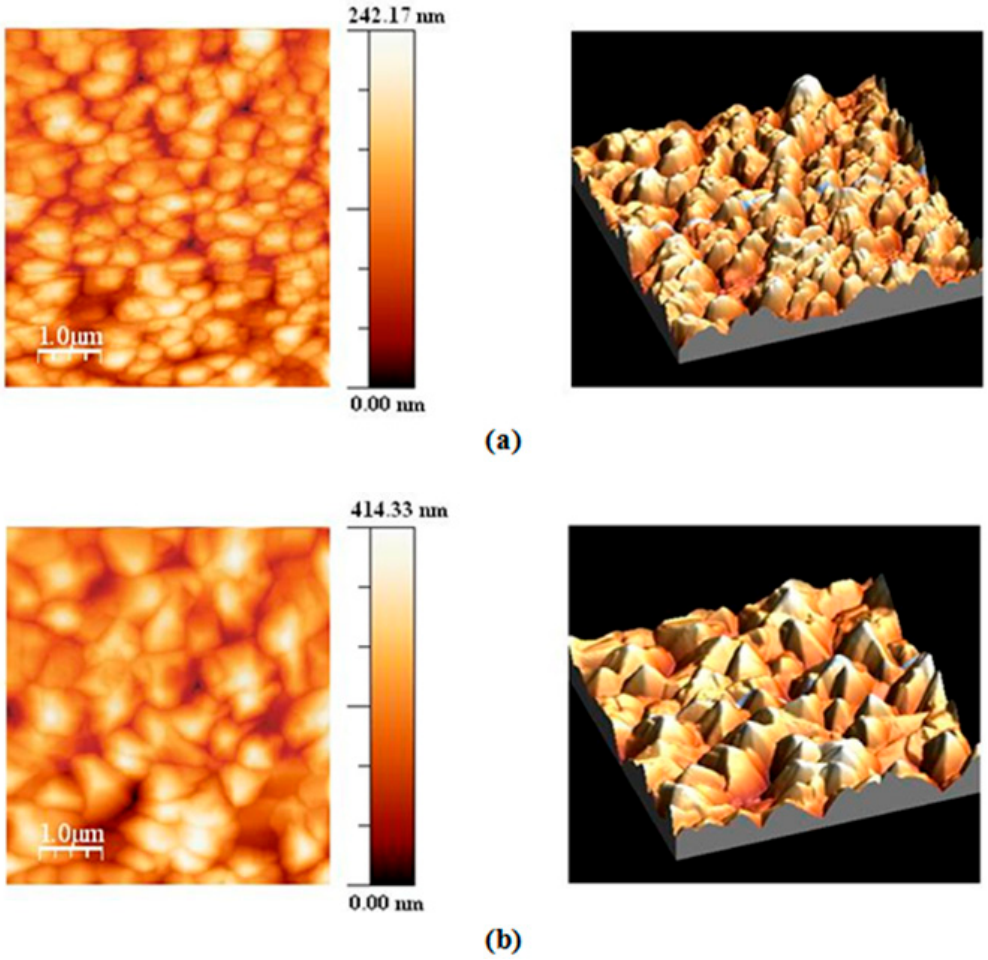

Figure 4. Two-dimensional and three-dimensional AFM images of $Zn_{1-x}Ni_xO$ thin films with content of Ni: (**a**) x = 0.02; (**b**) x = 0.06.

Figure 5 shows the transmittance spectra of $Zn_{1-x}Ni_xO$ thin films deposited on glass and SiO_2 substrates. All investigated $Zn_{1-x}Ni_xO$ films show a sharp absorption edge due to the fundamental absorption of zinc oxide. At the same time, the optical absorption edge of $Zn_{1-x}Ni_xO$ thin films shows a complex dependence on the nickel content. After Ni doping, the absorption edge shifts to the short-wavelength region for x = 0.02 and to the long-wavelength region of the spectrum for films with x > 0.02. The band gap Eg of the films was calculated by us by plotting the graph $(\alpha h\nu)^2$ as a function of the photon energy ($h\nu$). The value of Eg was determined by extrapolation of the linear part $(\alpha h\nu)^2$ on the energy axis. As can be seen from Figure 6, the calculated values of Eg increase with increasing Ni content up to x = 0.02 and decrease at x > 0.02. A more complex nature of the Eg(x) dependence, but very similar to that shown in Figure 6, was reported for nanoparticles [37] and $Zn_{1-x}Ni_xO$ nanoclusters [38]. The sinusoidal behaviour of Eg was also found on ZnO thin films doped with Ni [39]. Other studies have shown a decrease in Eg at low Ni concentrations and an increase in Eg at higher Ni concentrations [38,40]. Many research groups report data [30,32,41] on the observation of only a decrease in Eg with increasing x. This behaviour of Eg(x) can be caused by the formation of the Ni defect energy level. In addition, the Zni impurity creates shallow donor levels, which can lead to a decrease in the band gap of ZnO. According to studies [40], the decrease in Eg with increasing Ni content for sputtered thin films can be related to structural defects that can create localised states in the band gap. This decrease in the Eg is attributed mainly due to the s, p–d exchange interactions between band electrons and d electrons associated with the doped Ni^{2+} cations [40,42].

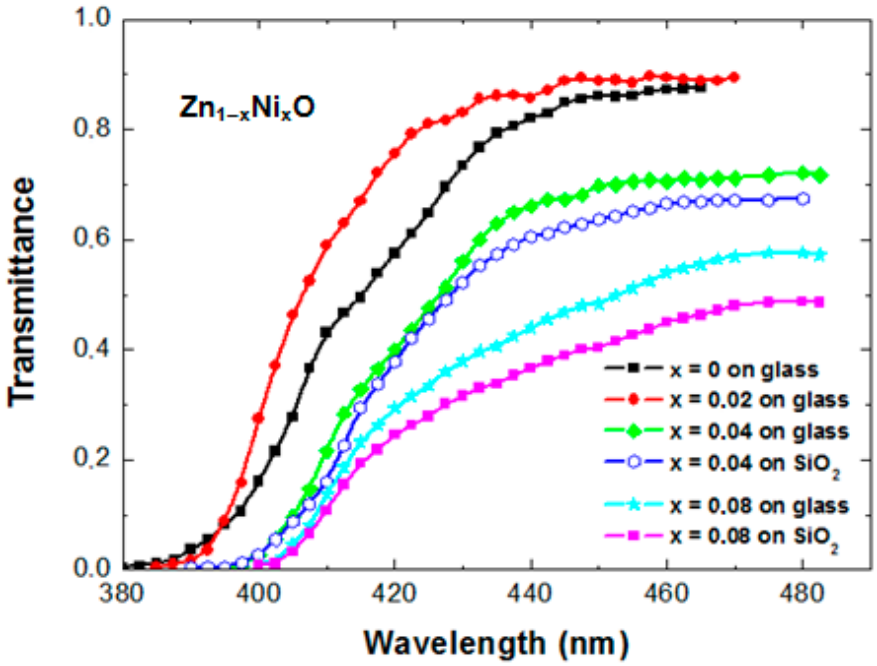

Figure 5. Transmittance spectra of $Zn_{1-x}Ni_xO$ thin films on different substrates near the absorption edge.

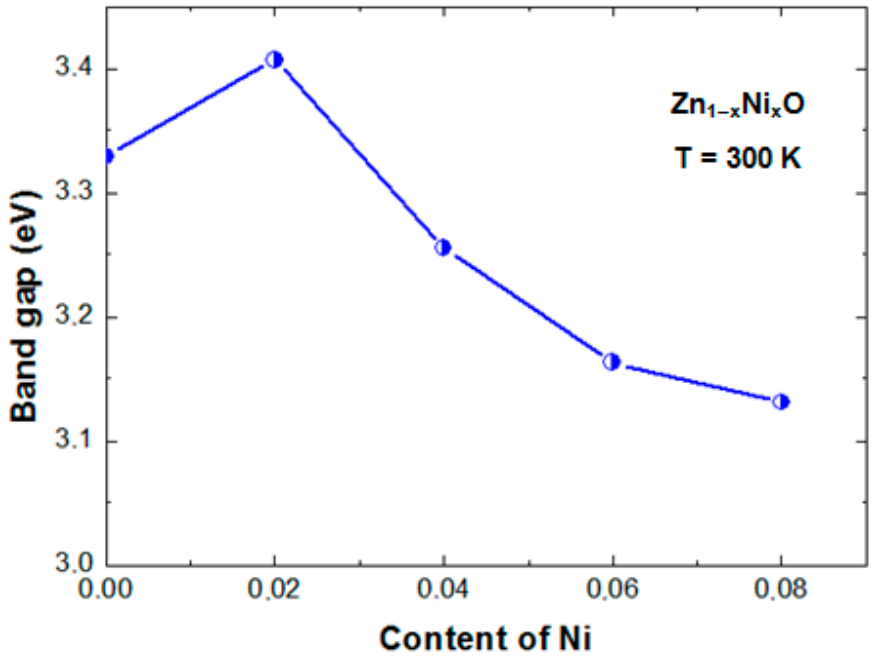

Figure 6. The optical band gap of $Zn_{1-x}Ni_xO$ thin films as a function of Ni content (x).

The initial increase in band gap from x = 0 to 0.02 the authors of the paper [37] have attributed to the s, p–d spin exchange interaction between the band carriers and localised spin of the transition metal ions. At the same time, the authors of the paper [43] have attributed this increase to the improvement of the crystalline structure of the films. Because of the nanostructured character of the prepared $Zn_{1-x}Ni_xO$ films according to the demonstrated above TEM and AFM images the same mechanisms can be applied also to explain the observed $E_g(x)$ dependence (Figure 6). Additional absorption below the absorption edge can be seen for slightly thicker $Zn_{1-x}Ni_xO$ films compared to those we used for the analysis of the absorption edge. From Figure 7 we can see in the transmit-

tance spectrum of $Zn_{0.96}Ni_{0.04}O$ film three absorption bands in the wavelength range 480–2000 nm. The absorption peaks identified in the long-wavelength region of the spectrum are caused by d–d transitions in tetrahedrally coordinated Ni^{2+} ions. The observed peaks can be attributed to $^3T_1(F) \rightarrow {}^1T_1(G)$, $^3T_1(F) \rightarrow {}^1T_1(D)$ and $^3T_1(F) \rightarrow {}^3T_1(P)$ transitions of the Ni^{2+} ions [44–47].

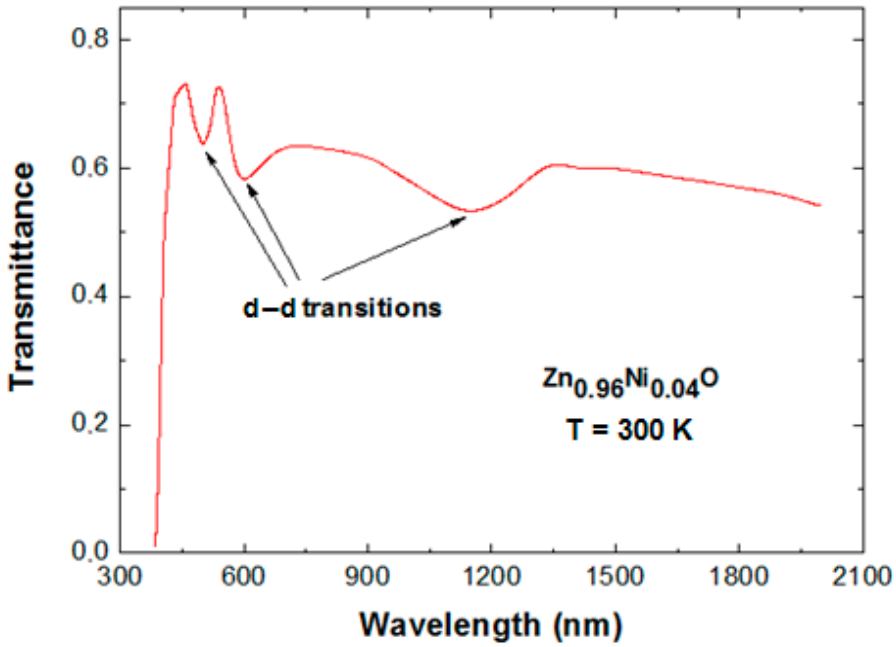

Figure 7. The d–d transitions of Ni^{2+} ions in transmittance spectrum of $Zn_{0.96}Ni_{0.04}O$ thin film.

The room temperature photoluminescence spectra of the $Zn_{1-x}Ni_xO$ thin films are shown in Figure 8. For all samples, an intense emission band at 380 nm is observed in the PL spectrum. This typical emission occurs in all studied films because of the near-band edge emission due to exciton-related transitions. The energy position of this band directly depends on the nickel content and is in good agreement with the results obtained from the optical absorption spectra. The energy position of this band directly depends on the nickel content and is in good agreement with the results obtained from the optical absorption spectra. The second emission peak near 460 nm is due to various vacancies and defect states. An increase in the concentration of nickel in thin films leads to broadened and a slight decrease in its intensity. Gao et al. [30] discussed possible manifestation of the six intrinsic defects in this region such as: interstitial oxygen, antisite oxygen, oxygen vacancy, interstitial zinc, antisite zinc and zinc vacancy.

The magneto-optical Faraday effect combines and synthesises two areas of physics—optics and magnetism. This effect occupies an important place in the study of the magneto-optical properties and the magnetic subsystem of various materials, in particular, DMS. The magnitude of the Faraday effect in DMS is directly related to the exchange interaction between the band states of electrons (holes) and localised d-(f−) electrons of magnetic ions and is proportional to the magnetisation of the magnetic subsystem. To our best knowledge, the magneto-optical Faraday effect was negligible for Ni-doped zinc oxides [43]. Figure 9 shows the spectral dependence of the Faraday rotation in $Zn_{1-x}Ni_xO$ thin films. The increase in the Faraday rotation in the region of the absorption edge is clearly observed with the increase in Ni content. As noted above, for DMS materials, the exchange interaction between band carriers and magnetic ions (s, p–d exchange interaction) leads to a strong increase in the Faraday rotation [48,49].

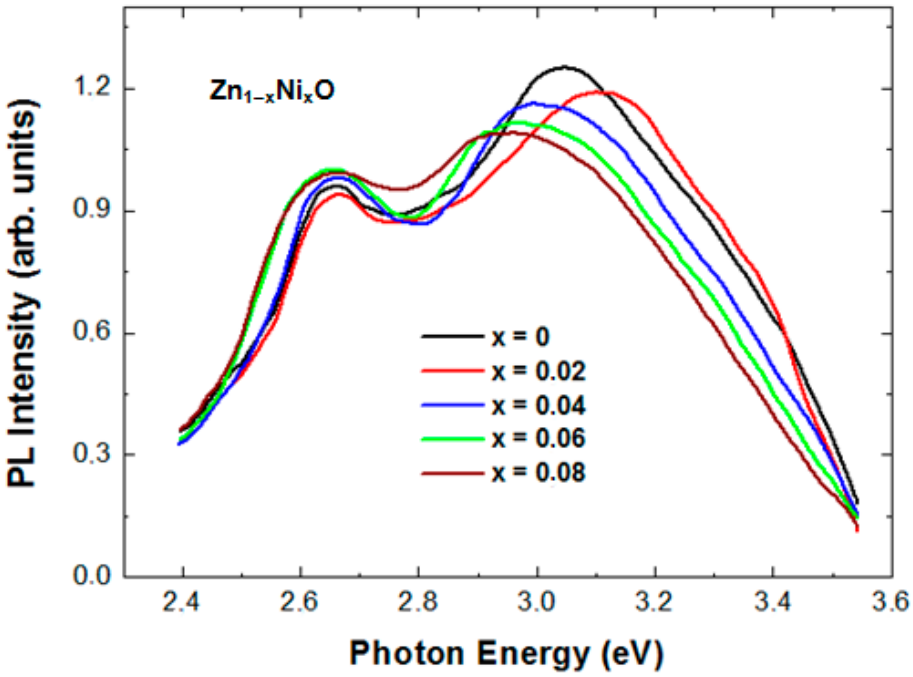

Figure 8. PL spectra of Ni-doped ZnO thin films with different Ni content.

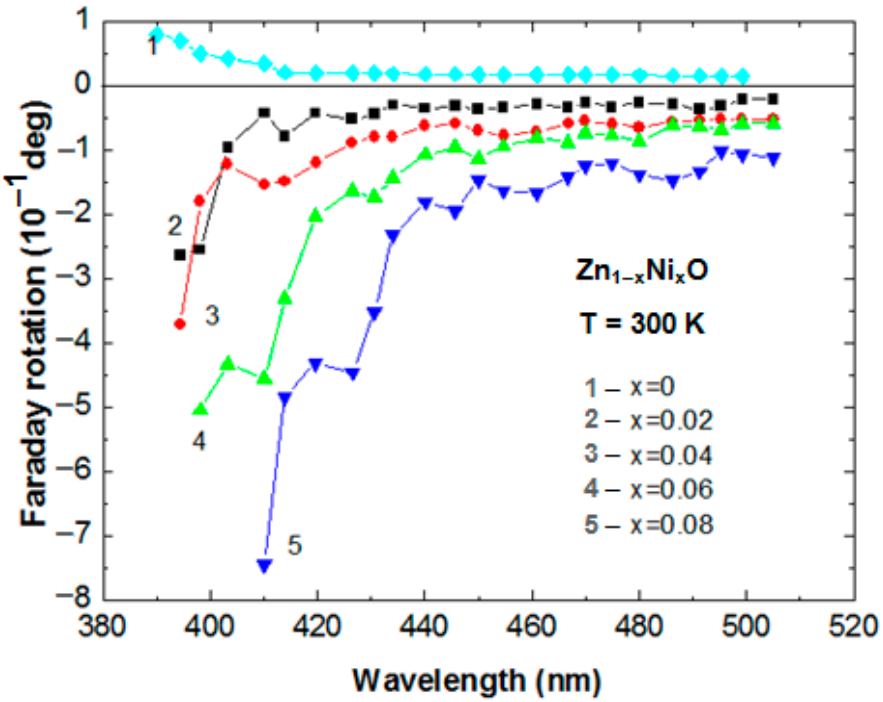

Figure 9. The Faraday rotation spectra as function of wavelength in $Zn_{1-x}Ni_xO$ thin films on glass substrate.

The ratio of angle θ_F to the product magnetic field B and sample thickness d is known as the Verdet constant (V):

$$V = \frac{\theta_F}{B\,d} \tag{4}$$

In accordance with to the microscopic model of the magneto-optical Faraday effect in bulk DMS [49,50] the Verdet constant as a function of photon energy hν can be expressed as:

$$V(h\nu) = Z \cdot f(X) + C \cdot Y \cdot g(X), \quad (5)$$

where X = E/Eg, Eg is the band-gap energy, E is photon energy and Z, C and Y are fitting parameters. The function f(X) has a positive sign, while the function g(X) is negative and characterises the "pure" Zeeman and exchange contributions, respectively. Therefore, there is competition between two contributions with opposite signs depending on the temperature and the content of Ni in the studied material.

The competition between diamagnetic and paramagnetic states should also be detected in the $Zn_{1-x}Ni_xO$ thin films studied by us. In fact, the enhancement of the Faraday rotation and changes in its spectral dependence are due to the positive and negative parts due to the contribution of the pure Zeeman and s, p–d exchange interactions, respectively. As a result, competition between these two contributions with opposite signs leads to the negative sign and the observed enhancement of the Faraday rotation in the Ni-doped ZnO thin films.

Additional information about the behaviour of the magnetic subsystem of $Zn_{1-x}Ni_xO$ thin films is provided by the study of the dependence of the Faraday rotation on the magnetic field. On the basis of such studies, we discovered features caused by an increase in the Ni content. For the films with $x \geq 4\%$ and in magnetic fields above 0.7 T, a clear saturation effect was observed on the $\theta_F(B)$ dependence. In addition, a detailed analysis of many $\theta_F(B)$ curves of all studied samples made it possible to find a magnetic hysteresis loop at room temperature, starting with the composition of $Zn_{0.96}Ni_{0.04}O$ (Figure 10). On the contrary, the observed linear dependence of $\theta_F(B)$ and the absence of hysteresis for the $Zn_{0.98}Ni_{0.02}O$ film indicates paramagnetism in these samples. The revealed results of the magnetic behaviour can be explained in terms of the magnetic polaron model (BMP).

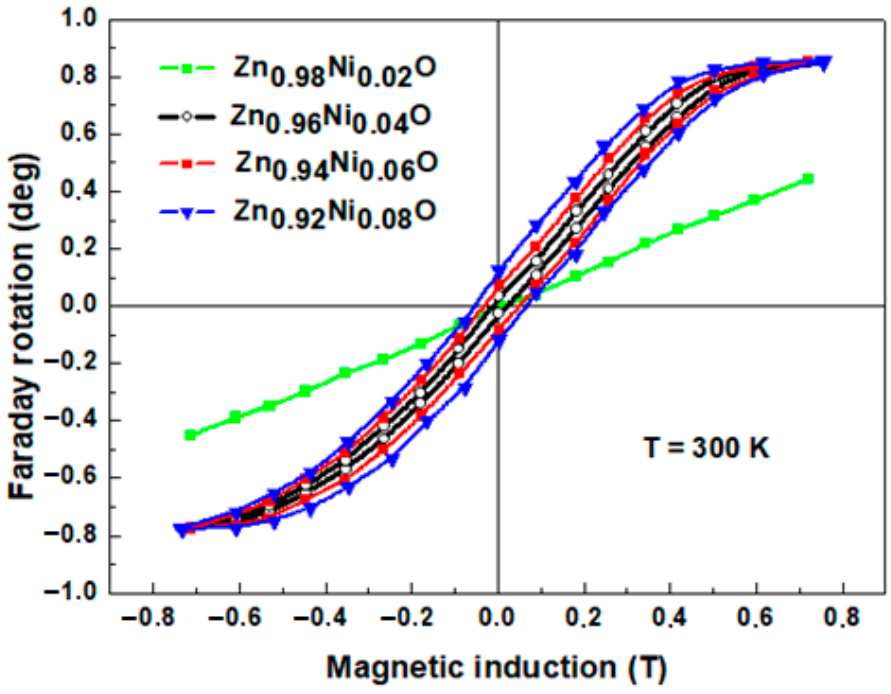

Figure 10. Magnetic field dependence of the Faraday rotation in $Zn_{1-x}Ni_xO$ thin films at room temperature.

According to works [51,52], the coexistence of O vacancies in ZnO lattices and Ni doping does not form secondary magnetic phases (clusters of Ni metal and nickel oxide). The magnetic properties of such an alloyed system are exclusively internal. In this case, in the BMP model, intrinsic ferromagnetism is caused by electrons captured by donor

defects (for example, oxygen vacancies), which occupy extended orbits and, overlapping, form a spin-split impurity zone with localised spins of transition Ni^{2+} ions [52,53]. This is consistent with the results by the authors [54,55], where the increasing density of oxygen vacancies ensured the formation of BMP and led to an increase in ferromagnetism.

From obtained results of the FR and PL investigations, we suggest that increasing the doping level of TM elements and defect concentration in the ZnO films results in increasing ferromagnetic ordering.

4. Conclusions

The $Zn_{1-x}Ni_xO$ thin films with $0 \leq x \leq 0.08$ were prepared successfully using by RF reactive sputtering technique on quartz, sapphire and glass substrates at room temperature. XRD analysis of $Zn_{1-x}Ni_xO$ thin films showed that the incorporation of nickel ions into the ZnO did not change the hexagonal wurtzite structure of the lattice with the preferred orientation of their growth along the (002) axis with good crystallinity.

It is observed from AFM images that the surface morphology of the $Zn_{1-x}Ni_xO$ thin films is characterised by a mixture of granular and columnar microstructures and growth perpendicular to the surface along the z-direction. The increase in the content of Ni leads to an increase in the root mean square values of the surface roughness.

The absorption edge shifts to low wavelengths (blue shift) with an increase in Ni content up to x = 0.02 and shifts to higher wavelengths (red shift) with an increase in Ni content for x > 0.02. The absorption measurement in the wavelength range 350–2100 nm shows absorption bands associated with the d–d electrons transition of Ni^{2+} within the tetrahedral symmetry. The two emission peaks in room temperature PL spectra are ascribed to exciton-related transitions and broadened intensive emission associated with vacancy or defect states. Changes in spectral dependence of the Faraday rotation angle and its negative sign are due to s, p–d exchange interaction between band carriers and spins of magnetic ions in $Zn_{1-x}Ni_xO$ thin films. Magnetic field dependence of Faraday rotation confirmed ferromagnetic behaviour in $Zn_{1-x}Ni_xO$ films with increasing Ni content higher than 2% at room temperature.

Author Contributions: Conceptualisation, I.S.; methodology, O.K. and I.H.; software, A.S.; validation, I.S., O.D. and A.S.; formal analysis, G.K.; investigation, I.S. and A.D.; resources, I.S.; data curation, A.P. and O.D.; writing—original draft preparation, I.S., O.K. and I.H.; writing—review and editing, I.S. and O.K.; visualisation, A.S. and A.P.; supervision, I.S.; project administration, I.S. All authors have read and agreed to the published version of the manuscript.

Funding: This work has been supported in part by grant No. DR/0120U102217 from the Ministry of Education and Science of Ukraine.

Institutional Review Board Statement: Not applicable.

Informed Consent Statement: Not applicable.

Data Availability Statement: Not applicable.

Acknowledgments: The authors would like to thank Jaime de Sousa from "Nanotec Electronica" for help in performing of AFM analysis. Ihor Stolyarchuk acknowledges the support in the frames of the Award of Iwan Wyhowski of the Centre for East European Studies at Warsaw University. Ihor Stolyarchuk and Ivan Hadzaman acknowledge the support in the frames of the IEEE program "Magnetism for Ukraine 2022" (grant 9918).

Conflicts of Interest: The authors declare that they have no conflict of interest.

References

1. Dietl, T.; Ohno, H.; Matsukura, M.; Cibert, J.; Ferrand, D. Zener model description of ferromagnetism in zinc-blende magnetic semiconductors. *Science* **2000**, *287*, 1019–1022. [CrossRef]
2. Sato, K.; Katayama-Yoshida, H. Ferromagnetism in a transition metal atom doped ZnO. *Phys. E* **2001**, *10*, 251–255. [CrossRef]
3. Sharma, P.; Gupta, A.; Owens, F.J.; Inoue, A.; Rao, K.V. Room temperature spintronic material—Mn-doped ZnO revisited. *J. Magn. Magn. Mater.* **2004**, *282*, 115–121. [CrossRef]

4. Kim, Y.M.; Yoon, M.; Park, I.-W.; Lyou, J.H. Synthesis and magnetic properties of $Zn_{1-x}Mn_xO$ films prepared by the sol–gel method. *Solid State Commun.* **2004**, *129*, 175–178. [CrossRef]
5. Diaconu, M.; Schmidt, H.; Hochmuth, H.; Lorenz, M.; Benndorf, G.; Lenzner, J.; Spemann, D.; Setzer, A.; Nielsen, K.-W.; Esquinazi, P.; et al. UV optical properties of ferromagnetic Mn-doped ZnO thin films grown by PLD. *Thin Solid Films* **2005**, *486*, 117–121. [CrossRef]
6. Joseph, D.P.; Kumar, G.S.; Venkateswaran, C. Structural, magnetic and optical studies of Zn 0.95 Mn 0.05 O DMS. *Mater. Lett.* **2005**, *59*, 2720–2724. [CrossRef]
7. Liu, C.; Xiao, B.; Yun, F.; Lee, H.; Ozgur, U.; Moon, Y.T.; Morkoc, H.; Abouzaid, M.; Ruterana, P. Effect of N doping on magnetic properties of (Zn, Mn)O thin films deposited by radio frequency magnetron sputtering. *Superlattices Microstruct.* **2006**, *39*, 124–129. [CrossRef]
8. Assadi, M.H.N.; Zhang, Y.B.; Li, S. N codoping induced ferromagnetism in ZnO: Co (10 1^{-} 0) thin films. *J. Appl. Phys.* **2009**, *106*, 093911. [CrossRef]
9. Yang, S.; Man, B.Y.; Liu, M.; Chen, C.S.; Gao, X.G.; Wang, C.C.; Hu, B. Structural, optical and magnetic properties of Zn1−xCoxO dilute magnetic semiconductors thin films by pulsed laser deposition. *Phys. B* **2010**, *405*, 4027–4031. [CrossRef]
10. Fukumura, T.; Jin, Z.; Kawasaki, M.; Shono, T.; Hasegava, T.; Koshihara, S.; Koinuma, H. Magnetic properties of Mn-doped ZnO. *Appl. Phys. Lett.* **2001**, *78*, 958–960. [CrossRef]
11. Ueda, K.; Tabata, H.; Kavai, T. Magnetic and electric properties of transition-metal-doped ZnO films. *Appl. Phys. Lett.* **2001**, *79*, 988–990. [CrossRef]
12. Kane, M.H.; Shalini, K.; Summers, C.J.; Varatharajan, R.; Nause, J.; Vestal, C.R.; Zhang, Z.J.; Ferguson, I.T. Electro-optical effect in ZnO:Mn thin films prepared by Xe sputtering. *J. Appl. Phys.* **2005**, *97*, 023906. [CrossRef]
13. Alaria, J.; Turek, P.; Bernard, M.; Bouloudenine, M.; Berbadj, A.; Brihi, N.; Schmerber, G.; Colis, S.; Dinia, A. No ferromagnetism in Mn doped ZnO semiconductors. *Chem. Phys. Lett.* **2005**, *415*, 337–341. [CrossRef]
14. Wakano, T.; Fujimura, N.; Morinaga, Y.; Abe, N.; Ito, T. Magnetic and magneto-transport properties of ZnO: Ni films. *Phys. E* **2001**, *10*, 260–264. [CrossRef]
15. Basri, S.H.; Abd Majid, W.H.; Talik, N.A.; Mohd Sarjidan, M.A. Tailoring electronics structure, electrical and magnetic properties of synthesized transition metal (Ni)-doped ZnO thin film. *J. Alloys Compd.* **2018**, *769*, 640–648. [CrossRef]
16. Anbuselvan, D.; Nilavazhagan, S.; Santhanam, A.; Chidhambaram, N.; Gunavathy, K.V.; Ahamad, T.; Alshehri, S.M. Room temperature ferromagnetic behavior of nickel-doped zinc oxide dilute magnetic semiconductor for spintronics applications. *Phys. E* **2021**, *129*, 114665–114668. [CrossRef]
17. Liu, E.; Xiao, P.; Chen, J.S.; Lim, B.C.; Li, L. Ni doped ZnO thin films for diluted magnetic semiconductor materials. *Curr. Appl. Phys.* **2008**, *8*, 408–411. [CrossRef]
18. Yin, Z.G.; Chen, N.; Yang, F.; Song, S.L.; Chai, C.L.; Zhang, J.; Qian, H.J.; Ibrahim, K. Structural, magnetic properties and photoemission study of Ni-doped ZnO. *Solid State Commun.* **2005**, *135*, 430–433. [CrossRef]
19. Savchuk, A.I.; Gorley, P.N.; Khomyak, V.V.; Ulyanytsky, K.S.; Bilichuk, S.V.; Perrone, A.; Nikitin, P.I. ZnO-based semimagnetic semiconductors: Growth and magnetism aspects. *Mater. Sci. Engine B* **2004**, *109*, 196–199. [CrossRef]
20. Savchuk, A.I.; Fediv, V.I.; Savchuk, S.A.; Perrone, A. Growth and characterization of ZnMnO thin films. *Superlattices Microstruct.* **2005**, *38*, 421–427. [CrossRef]
21. Savchuk, A.I.; Fediv, V.I.; Kleto, G.I.; Krychun, S.V.; Savchuk, S.A. Optical and magneto-optical properties of ZnMnO and ZnMnFeO single crystals and thin films. *Phys. Status Solidi A* **2007**, *204*, 106–111. [CrossRef]
22. Savchuk, A.I.; Makhniy, V.P.; Fediv, V.I.; Kleto, G.I.; Savchuk, S.A.; Perrone, A.; Cultrera, L. Effects of codoping in ZnO-based semimagnetic semiconductor thin films. *IOP Conf. Ser. Mater. Sci. Engine* **2010**, *8*, 012042. [CrossRef]
23. Crassee, I.; Levallois, J.; Walter, A.L.; Ostler, M.; Bostwick, A.; Rotenberg, E.; Seyller, T.; van der Marel, D.; Kuzmenko, A.B. Giant Faraday rotation in single- and multilayer grapheme. *Nat. Phys.* **2011**, *7*, 48–51. [CrossRef]
24. Savchuk, A.I.; Stolyarchuk, I.D.; Makoviy, V.V.; Savchuk, O.A. Magneto-optical Faraday rotation of semiconductor nanoparticles embedded in dielectric matrices. *Appl. Opt.* **2014**, *53*, B22–B26. [CrossRef]
25. Cullity, B.D. *Elements of X-ray Diffractions*, 2nd ed.; Addison-Wesley Publishing Company INC.: San Francisco, CA, USA, 1978; 569p.
26. Rambu, A.P.; Ursu, L.; Iftimie, N.; Nica, V.; Dobromir, M.; Iacomi, F. Study on Ni-doped ZnO films as gas sensors. *Appl. Surf. Sci.* **2013**, *280*, 598–604. [CrossRef]
27. Venkatachalam, S.; Iida, Y.; Kanno, Y. Preparation and characterization of Al doped ZnO thin films by PLD. *Superlattices Microstruct.* **2008**, *44*, 127–135. [CrossRef]
28. Cullity, B.D.; Rstock, S. *Elements of X-ray Diffraction*, 3rd ed.; Prentice-Hall: New York, NY, USA, 2001; 696p.
29. Shannon, R.D. Revised effective ionic radii and systematic studies of interatomic distances in halides and chalcogenides. *Acta Crystallogr. Sect. A* **1976**, *32*, 751–767. [CrossRef]
30. Gao, F.; Tan, L.X.; Wu, Z.H.; Liu, X.Y. Microstructural and optical properties of ZnO/(Ni) thin films prepared by DC magnetron sputtering. *J. Alloys Compd.* **2009**, *484*, 489–493. [CrossRef]
31. Siddheswaran, R.; Netrvalova, M.; Savkova, J.; Novak, P.; Ocenasek, J.; Sutta, P.; Kovac, J., Jr.; Jayavel, R. Reactive magnetron sputtering of Ni doped ZnO thin film: Investigation of optical, structural, mechanical and magnetic properties. *J. Alloys Compd.* **2015**, *636*, 85–92. [CrossRef]

32. Jlassi, M.; Sta, I.; Hajji, M.; Ezzaouia, H. Effect of nickel doping on physical properties of zinc oxide thin films prepared by the spray pyrolysis method. *Appl. Surf. Sci.* **2014**, *301*, 216–224. [CrossRef]
33. Hu, D.; Liu, Y.J.; Li, H.S.; Cai, X.Y.; Yan, X.L.; Wang, Y.D. Effect of nickel doping on structural, morphological and optical properties of sol–gel spin coated ZnO films. *Mater. Technol.* **2012**, *27*, 243–248. [CrossRef]
34. Mahbubur Rahman, M.; Awaltanova, E.; Amri, A.; Altarawneh, M.; Hossain Md, A.; Zhao, X.; Liew, W.Y.H.; Minakshi, M.; Yin, C.-Y.; Veder, J.-P.; et al. A holistic analysis of surface, chemical bonding states and mechanical properties of sol-gel synthesized CoZn-oxide coatings complemented by finite element modeling. *Ceram. Int.* **2019**, *45*, 10882–10898. [CrossRef]
35. Siddheswaran, R.; Mangalaraja, R.V.; Tijerina, E.P.; Menchaca, J.-L.; Melendrez, M.F.; Avila, R.E.; Jeayanthi, C.E.; Gomez, M.E. Fabrication and characterization of a diluted magnetic semiconducting TM co-doped Al:ZnO (TM=Co, Ni) thin films by sol-gel spin coating method. *Spectrochim. Acta A* **2013**, *106*, 118–123. [CrossRef]
36. Stamataki, M.; Tsamakis, D.; Xanthakis, J.P.; Ali, H.A.; Esmaili-Sardari, S.; Iliadis, A.A. Electrical characterization of Cr Schottky contacts on undoped and Ni-doped p-ZnO films grown by pulsed laser deposition on Si (100) substrates. *Microelectron. Engine* **2013**, *104*, 95–99. [CrossRef]
37. Gopalakrishnan, R.; Muthukumaran, S. Nanostructure, optical and photoluminescence properties of $Zn_{1-x}Ni_xO$ nanoclusters by co-precipitation method. *J. Mater. Sci. Mater. Electron.* **2013**, *24*, 1069–1080. [CrossRef]
38. Fabbiyola, S.; Sailaja, V.; John Kennedy, L.; Bououdina, M.; Judith Vijaya, J. Optical and magnetic properties of Ni-doped ZnO nanoparticles. *J. Alloys Comp.* **2017**, *694*, 522. [CrossRef]
39. Abed, S.; Aida, M.S.; Bouchouit, K.; Arbaui, A.; Iliopoulos, K.; Sahraoui, B. Nonlinear optical and electrical properties of ZnO doped Ni Thin Films obtained using spray ultrasonic technique. *Opt. Mater.* **2011**, *33*, 968–972. [CrossRef]
40. Reddy, M.R.; Sugiyama, M.; Reddy, K.T.R. Ni-Doping Effect on the Structural and Optical Properties of Sprayed ZnO Thin Films. *Adv. Mater. Res.* **2013**, *602–604*, 1423–1426. [CrossRef]
41. Mishra, P.K.; Amin, R.; Biring, S.; Sen, S. Structural and optical studies of Ni-doped ZnO. *AIP Conf. Proc.* **2019**, *2100*, 020121.
42. Ali, H.; Alsmadi, A.M.; Salameh, B.; Mathai, M.; Shatnawi, M.; Hadia, N.M.A.; Ibrahim, E.M.M. Influence of nickel doping on the energy band gap, luminescence, and magnetic order of spray deposited nanostructured ZnO thin films. *J. Alloys Compd.* **2018**, *816*, 152538. [CrossRef]
43. Fiaz Khan, M.; Siraj, K.; Anwar, M.S.; Irshad, M.; Hussain, J.; Faiz, H.; Majeed, S.; Dosmailov, M.; Patek, J.; Pedarnig, J.D.; et al. 700 keV Ni+2 ions induced modification in structural, surface, magneto-optic and optical properties of ZnO thin films. *Nucl. Instrum. Methods Phys. Res. B* **2016**, *368*, 45–49. [CrossRef]
44. Weakliem, H.A. Optical Spectra of Ni2+, Co2+, and Cu2+ in Tetrahedral Sites in Crystals. *J. Chem. Phys.* **1962**, *36*, 2117–2140. [CrossRef]
45. Singh, S.; Rama, N.; Rao, M.S. Ramachandra. Influence of d-d transition bands on electrical resistivity in Ni doped polycrystalline ZnO. *Appl. Phys. Lett.* **2006**, *88*, 222111. [CrossRef]
46. Elilarassi, R.; Chandrasekaran, G. Synthesis, structural and optical characterization of Ni-doped ZnO nanoparticles. *J Mater. Sci. Mater. Electron.* **2011**, *22*, 751–756. [CrossRef]
47. Qu, B.; Liu, M.; Zhou, R.; Jiang, Y.; Wang, L. The predictability of the ground state of 3dn transition metal ion as luminescent centers in the tetrahedral sites in inorganic compounds. *J. Lumin.* **2022**, *247*, 118919. [CrossRef]
48. Nikitin, P.I.; Savchuk, A.I. The Faraday effect in semimagnetic semiconductors. *Sov. Phys. Usp.* **1990**, *33*, 974–989. [CrossRef]
49. Buss, C.; Hugonnard-Bruyere, S.; Frey, R.; Flytzanis, C. Theory of Faraday rotation in semimagnetic semiconductors. *Solid State Commun.* **1994**, *92*, 929–933. [CrossRef]
50. Huggonard-Bruyere, S.; Buss, C.; Vouilloz, F.; Frey, R.; Flytzanis, C. Faraday-rotation spectra of semimagnetic semiconductors. *Phys. Rev. B* **1994**, *50*, 2200–2207. [CrossRef]
51. Hou, Q.; Wang, Z. First-principle study of the effects of Ni doping and point vacancy on the magnetic and absorption spectrum and itinerant electron properties of ZnO. *Solid State Commun.* **2022**, *352*, 114813. [CrossRef]
52. Chithira, P.R.; John, T.T. Defect and dopant induced room temperature ferromagnetism in Ni doped ZnO nanoparticles. *J. Alloys Compd.* **2018**, *766*, 572–583. [CrossRef]
53. Coey, J.M.D.; Venkatesan, M.; Fitzgerald, C.B. Donor impurity band exchange indilute ferromagnetic oxides. *Nat. Mater.* **2005**, *4*, 173–179. [CrossRef] [PubMed]
54. Iqbal, J.; Wang, B.; Liu, X.; Yu, D.; He, B.; Yu, R. Oxygen-vacancy-induced green emission and room-temperature ferromagnetism in Ni-doped ZnO nanorods. *New J. Phys.* **2009**, *11*, 063009. [CrossRef]
55. Kumar, P.; Malik, H.K.; Asokan, K. Tuning of optical bandgap and magnetization of C-implanted ZnO thin films. *EPL Europhy. Lett.* **2015**, *110*, 67006. [CrossRef]